Article:
Wang, Y., Chen, C., Zheng, H. et al. (2023) Performance of indoor small-cell networks under interior wall penetration losses. IEEE Internet of Things Journal, 10 (12). pp. 10907-10915. ISSN: 2327-4662

https://doi.org/10.1109/jiot.2023.3241759

Performance of Indoor Small-Cell Networks under Interior Wall Penetration Losses

Yunbai Wang, Chen Chen, Hui Zheng, Xiaoli Chu

***Abstract*—The performance of indoor small-cell networks (SCNs) is affected by the indoor environment, such as walls, blockages, etc. In this paper, we investigate the effect of interior wall attenuation on the performance of an indoor SCN. Specifically, the spatial distribution of interior walls is modelled based on the random shape theory and the indoor base stations (BSs) are distributed following a homogeneous Poisson point process. The channel model includes the path loss, Rayleigh fading, and wall attenuation. We analytically derive the downlink coverage probability under the strongest received signal user association strategy, which is validated by Monte Carlo simulations for three typical interior wall layouts (i.e., random layout, binary orientation layout, and Manhattan grid). The analytical results show that for a given density of interior walls and signal strength attenuation per wall, there is an optimal BS density that maximises the coverage probability, and the optimal BS density increases as the wall attenuation increases.**

***Index Terms*—Indoor, small-cell network, stochastic geometry, coverage probability, wall blockage, user association strategy.**

I. Introduction

It is expected that the mobile traffic demand will grow at an annual rate of 47 % by 2030, with about 80% of traffic demand generated indoors [1], [2]. The indoor wireless capacity can be tremendously improved by the deployment of small cells with high spatial spectrum reuse, which can implement the existing networks [3]. The previous work on indoor wireless communication either ignored the effects of interior walls [2], [4] or focused on the line-of-sight (LOS) probabilities of indoor transmission links [5], [6] and wall reflection [7]. In this paper, we endeavour to analytically evaluate the coverage performance of indoor small-cell networks (SCNs) using stochastic geometry, considering the effects of interior walls, and shed new insights into practical deployment of indoor small cells.

A. Related Works

In order to effectively evaluate the performance of SCNs, stochastic geometry is widely used to model the locations of base stations (BSs). In [8], the locations of BSs were distributed following a homogeneous Poisson point process (HPPP) on a two dimensional (2-D) plane, and the closed-form expression of coverage probability was derived. In [9], [10], multi-tier heterogeneous networks (HetNets) were modelled using stochastic geometry where BSs in each tier were distributed following an independent HPPP. However, these works oversimplified the path-loss model, without differentiating line-of-sight (LOS) and non-line-of-sight (NLOS) transmissions. The authors in [11]–[14] investigated the effect of LOS/NLOS propagation on the network performance of outdoor SCNs. Their results show that in the presence of blockages, the coverage probability of a single-tier SCN first increases and then decreases with the BS density [11]–[13], while that of a HetNet monotonically decreases with the small-cell BS density [14]. In [15]–[17], millimeter-wave SCNs were modelled and analysed taking into account the effects of blockages and antenna array gain. Nevertheless, the aforementioned works are not applicable to the analysis of indoor SCNs.

For indoor environments, the authors in [2], [5], [18], [19] studied the performance of SCNs considering the modelling of building structures. The authors in [18] developed a spatial model of in-building SCNs and investigated the correlated shadowing among the links passing through the walls and ceilings. In [5], the LOS probability was derived for practical indoor layouts with interior walls and ceilings, but indoor wireless coverage performance was not studied in [5], [18]. In [2], the authors developed a tractable SCN model for a multi-story building and investigated the influence of ceilings on the network coverage and capacity. In [19], the locations of indoor small-cel BSs in a building were modelled following a 3D PPP. However, these two studies ignored the effects of interior walls on the indoor wireless coverage.

Several papers [20]–[25] addressed the effects of interior walls on the coverage performance of indoor SCNs. In [20], the effects of different wall layouts were discussed. The authors in [21] analysed the effect of wall-angle distributions on indoor wireless communications. However, only the specific placements of BSs were considered and no tractable analytical expression of coverage probability was provided in [20], [21]. In [22], the authors derived the coverage probability of indoor SCNs with wall blockages based on the horizontal or vertical orientations of walls, but the interior walls were simply considered as impenetrable blockages. The interior wall attenuation was studied in [23], and the probability mass function of the number of penetrated walls was derived, where the wall layouts were modelled as regular grids. In [24] and [25], the authors derived the expression of coverage probability for indoor SCNs using stochastic geometry and incorporated the wall attenuation into the path-loss model under the nearest LOS and NLOS BS user association strategies (UASs), respectively, but these two UASs cannot guarantee that the user is

Yunbai Wang and Xiaoli Chu are with Department of Electronic and Electrical Engineering, the University of Sheffield, Sheffield, S1 4ET, UK. Chen Chen is with the Department of Electrical Engineering and Electronics, the University of Liverpool, Liverpool, L69 3GJ, UK. Hui Zheng is with the Department of Information and Communication Engineering, the University of Beijing Information Science and Technology, Beijing, CN.

This work was supported in part by the European Unions Horizon 2020 research and innovation programme under grant agreement No. 734798.

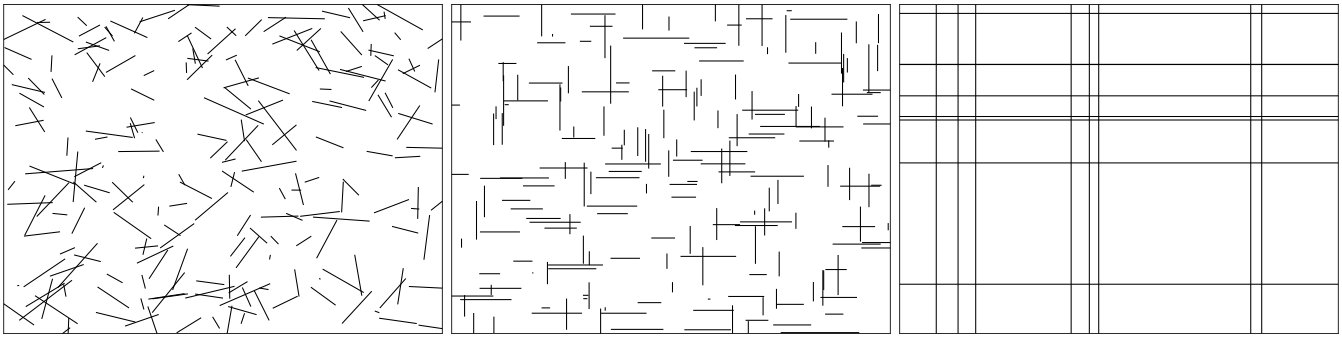

(a) (b) (c)

Fig. 1. Three typical wall layouts: (a) Random layout: the wall orientation ψ_k is randomly chosen in the range $[0, \pi)$, (b) Binary orientation layout: the wall orientation ψ_k is randomly chosen from $\{0, \frac{\pi}{2}\}$, and (c) Manhattan grid: the interior walls are generated by Manhattan Poisson line processes. These three scenarios are created with parameters that lead to the same average wall volume [20].

connected to the BS providing the strongest signal.

B. Contributions

The effect of interior wall attenuation on the coverage performance of an indoor SCN under the strongest received signal UAS has not been sufficiently studied. To fill this gap, in this paper, we investigate the downlink coverage performance of an indoor SCN considering interior wall attenuation. The main contributions of this paper are summarised as follows:

- We develop a stochastic geometry-based framework for indoor SCNs, where the indoor small-cell BSs are distributed following an HPPP. The interior walls are modelled by using the random shape theory [26], in which the interior walls are modelled as line segments with random lengths and orientations, and the centres of interior walls follow another HPPP.
- We propose an indoor channel model that includes the distance-dependent indoor path-loss, LOS probability, small-scale fading and wall attenuation.
- Based on the constructed system model, we derive the probability density function (PDF) of the distance from a typical user to its serving BS under the strongest received signal UAS, and use the PDF to derive a numerically tractable expression of the downlink coverage probability for the indoor SCN while considering the interior wall attenuation.
- The derived coverage probability is verified by Monte Carlo simulations for different interior wall attenuation, BS densities and wall densities. Besides, we compare the coverage probability of SCNs under three typical interior wall layouts: random layout, binary orentation layout and Manhatan grid, through simulations and obtain insights into the effect of interior wall attenuation on the downlink coverage probability.

C. Paper Organization

This paper is organized as follows. In Section II, the system model is introduced. In Section III, the expressions of Signal-to-Interference-plus-Noise Ratio (SINR) and downlink coverage probability are derived. In Section IV, the numerical results are discussed. In Section V, the conclusions and suggestions for future work are provided.

II. System Model

In this section, an indoor SCN model is presented, where the BSs are generated by an HPPP and three typical layouts of wall are considered. We propose a path-loss model consisting of the LOS probability, the large-scale path loss, the small-scale fading, and the wall attenuation.

A. Network Model

We consider an indoor area on a single floor represented by a 2-D plane. The locations of BSs are randomly distributed following an HPPP Φ with density μ. The locations of users are modelled following another independent HPPP Φ_{U}. Without loss of generality, the typical user is located at the centre of the considered area. We assume orthogonal time/frequency resource partitioning, and thus there is no intra-cell interference.

B. Wall Blockage Models

For indoor environments, three typical models of wall layouts are considered, as shown in Fig. 1. To generate interior walls for the random layout and binary orientation layout, we adopt the random shape theory to model the wall blockages. The centres of wall blockages are distributed on the 2-D plane following an HPPP Γ with density λ. The length of an arbitrary wall l_k is modelled following an arbitrary PDF $f_L(l_k)$ with mean L. The thickness of walls is neglected [20]. The orientation of an arbitrary wall is ψ_k, where $k \in \Gamma$.

For the random layout shown in Fig. 1(a), the wall orientation is randomly distributed in the range $[0, \pi)$. Accordingly, the average number of interior walls intersected with the i-th link is given by [25]

$$E[K_i] = \frac{2\lambda L}{\pi} d_i, \tag{1}$$

where K_i is the number of walls intersecting the i-th link and d_i is the length of the i-th link. For the binary orientation layout shown in Fig. 1(b), the wall orientation $\psi_k \in \{0, \frac{\pi}{2}\}$,

and the average number of interior walls intersected with the i-th link is given by [22]

$$E[K_i] = \frac{\lambda L}{2}(|\sin(\theta_i)| + |\cos(\theta_i)|)d_i, \tag{2}$$

where θ_i represents the angle between the i-th link and the horizontal axis.

The Manhattan grid layout shown in Fig. 1(c) can be obtained by two independent Manhattan Poisson line processes. Specifically, the centres of walls are distributed according to one-dimensional (1-D) PPPs along each axis with density λ'. The average number of interior walls intersected with the i-th link is given by [20]

$$E[K_i] = \lambda'(|\sin(\theta_i)| + |\cos(\theta_i)|)d_i. \tag{3}$$

To enable fair comparison, it is expected that the considered three wall layouts generate the same average wall volume, i.e., average length of all walls. To this end, the 1-D density λ' of Manhattan grid layout is set to $\lambda' = \frac{\lambda L}{2}$.

C. Path Loss Model

In this paper, we adopt the strongest received signal UAS. Each user connects to the BS providing the strongest downlink received signal, which means the serving BS can be either LOS or NLOS for the typical user. The path loss in our system model can be expressed as

$$L(d_i) = \begin{cases} \eta_0 d_i^{-\alpha}, & \text{if the link is LOS} \\ S_i^{\mathrm{N}} \eta_0 d_i^{-\alpha}, & \text{if the link is NLOS} \end{cases}, \tag{4}$$

where η_0 is the path loss at the reference distance of 1 m, α is the path-loss exponent and S_i^{N} is the wall attenuation for the i-th NLOS link. Although LOS and NLOS links typically have different path-loss exponents, the introduction of the wall attenuation into the path-loss model allows the same distance-based path-loss exponent α for LOS and NLOS links. The wall attenuation for the i-th NLOS link is $S_i^{\mathrm{N}} = \prod_{k=0}^{K_i} \omega = \omega^{K_i}$, where ω is the attenuation of each wall. Thereby, the number of walls intersecting with the i-link is essential for deriving the wall attenuation of NLOS links, and is affiliated with the layout of wall blockages.

III. Downlink Coverage Probability

In this section, we derive the downlink coverage probability for the random layout with wall orientation $\psi_k \in [0, \pi)$ for tractability. We provide simulation results of the coverage probabilities for the other two wall layouts in Section IV. Specifically, the typical user is served by the BS providing the strongest downlink received signal, where the link of user association should have the smallest path loss. Besides, the locations of wall blockages are assumed to be independent in this paper (the correlation of wall blockages is not considered).

In the scenario of random layout, where the uniformly distributed wall orientation $\psi_k \in [0, \pi)$, the probability of a link being LOS or NLOS is a Bernoulli random variable. The probability that the i-th link is in LOS condition is given by [11]

$$P_{\mathrm{L}}(d_i) = e^{-\frac{2\lambda L}{\pi} d_i} = e^{-\beta d_i}, \tag{5}$$

where $\beta = \frac{2\lambda L}{\pi}$. Accordingly, the probability that the i-th link is in NLOS condition is given by

$$P_{\mathrm{N}}(d_i) = 1 - P_{\mathrm{L}}(d_i) = 1 - e^{-\beta d_i}. \tag{6}$$

Therefore, the path loss model is expressed as

$$L_{\mathrm{R}}(d_i) \overset{(a)}{\approx} \begin{cases} \eta_0 d_i^{-\alpha}, & \text{with probability } P_{\mathrm{L}}(d_i) \\ \omega^{E[K_i]} \eta_0 d_i^{-\alpha}, & \text{with probability } P_{\mathrm{N}}(d_i) \end{cases}, \tag{7}$$

where step (a) is that, in the attenuation for the i-th NLOS link $S_i^{\mathrm{N}} = \omega^{K_i}$, the actual number of interior wall K_i is replaced by the average number of interior wall $E[K_i]$ for the purpose of mathematical tractability. Thus, the wall attenuation for the i-th NLOS link can be derived as $S_i^{\mathrm{N}} = \omega^{E[K_i]}$. This means that the wall attenuation of NLOS links can be characterized by the length of links.

Besides, the expression of SINR is expressed as

$$\begin{aligned} \mathrm{SINR} &= \frac{p_T h_j L(d_j)}{\sum\limits_{i \in \Phi / j, d_i \in (0, D)} p_T h_i L(d_i) + N_0} \\ &\approx \frac{p_T h_j L_{\mathrm{R}}(d_j)}{\sum\limits_{i \in \Phi_{\mathrm{L}} / j} p_T h_i L_{\mathrm{R}}(d_i) + \sum\limits_{i \in \Phi_{\mathrm{N}} / j} p_T h_i L_{\mathrm{R}}(d_i) + N_0} \\ &= \frac{p_T h_j L_{\mathrm{R}}(d_j)}{I_{\mathrm{L}} + I_{\mathrm{N}} + N_0}, \end{aligned} \tag{8}$$

where p_T represents the transmission power of a BS assuming all BSs have the same transmission power, D is the maximum length of links in the considered indoor scenario, N_0 is the additive white Gaussian noise (AWGN) power, d_j represents the length of j-th link between the typical user and its serving BS, h_i and h_j denote the power gains of Rayleigh fading for the j-th link and the i-th link, respectively, I_{L} and I_{N} denote the total interference powers received by the typical user from LOS and NLOS interference links, respectively. Φ_{L} denotes the set of LOS BSs and Φ_{N} denotes the set of NLOS BSs.

The coverage probability represents the probability that the SINR of the typical user is higher than a given threshold and is computed by

$$\begin{aligned} P_c(T) &= \mathbb{P}(\mathrm{SINR} > T) \\ &= P_c^{\mathrm{L}}(T) + P_c^{\mathrm{N}}(T) \\ &= \int_0^D \mathbb{P}\left[\frac{p_T h_j L_{\mathrm{R}}(d_{\mathrm{LOS}_j})}{I_{\mathrm{L}} + I_{\mathrm{N}} + N_0} > T\right] \hat{f}_{\mathrm{L}}(r)\mathrm{d}r \quad + \\ &\quad \int_0^D \mathbb{P}\left[\frac{p_T h_j L_{\mathrm{R}}(d_{\mathrm{NLOS}_j})}{I_{\mathrm{L}} + I_{\mathrm{N}} + N_0} > T\right] \hat{f}_{\mathrm{N}}(r)\mathrm{d}r, \end{aligned} \tag{9}$$

where T is the threshold of SINR, d_{LOS_j} and d_{NLOS_j} are the length of the LOS and NLOS serving links, respectively, r is the length of the serving link, $\hat{f}_{\mathrm{L}}(r)$ and $\hat{f}_{\mathrm{N}}(r)$ are the PDFs of the distance r from the typical user to its serving BS, when the serving BS is in LOS or NLOS conditions, respectively.

A. PDF of the Strongest Received Signal UAS

In this subsection, the distribution of the serving link is characterized. Under the strongest received signal UAS, the typical user is served by the BS providing the strongest

downlink received signal and thus the serving link has the largest value of $L_{\mathrm{R}}(d_i)$.

Lemma 1. *For the strongest received signal connectivity, the PDF of the typical user connecting to the nearest LOS BS at the distance r is derived as*

$$\hat{f}_{\mathrm{L}}(r) = e^{-\int_0^{r_1} P_{\mathrm{N}}(r)2\pi\mu t\mathrm{d}t} \times e^{-\int_0^{r} P_{\mathrm{L}}(r)2\pi\mu t\mathrm{d}t} \times P_{\mathrm{L}}(r)2\pi\mu r. \tag{10}$$

where r_1 represents the distance from the typical user to its nearest NLOS BS. The path loss of an NLOS link $L_{\mathrm{R}}(d_{\mathrm{NLOS}_i})$ is always smaller than the path loss of the serving LOS link $L_{\mathrm{R}}(r)$. Therefore, the minimum distance r_1 between the typical user and the NLOS BSs can be computed by

$$r_1 = r\omega^{\frac{E[K_i]}{\alpha}}. \tag{11}$$

Proof: See Appendix A. ∎

Substituting (5) and (6) into (10), $\hat{f}_{\mathrm{L}}(r)$ can be rewritten as

$$\hat{f}_{\mathrm{L}}(r) = 2\pi\mu r e^{-\beta r} \times e^{-2\pi\mu(\frac{1-e^{-\beta r}(1+\beta r)}{\beta^2})} \times e^{-2\pi\mu(\frac{r_1^2}{2}+\frac{e^{-\beta r_1}(1+\beta r_1)-1}{\beta^2})}. \tag{12}$$

Lemma 2. *For the strongest received signal connectivity, the PDF of the typical user connecting to the nearest NLOS BS at the distance r can be derived as*

$$\hat{f}_{\mathrm{N}}(r) = e^{-\int_0^{r_2} P_{\mathrm{L}}(r)2\pi\mu t\mathrm{d}t} \times e^{-\int_0^{r} P_{\mathrm{N}}(r)2\pi\mu t\mathrm{d}t} \times P_{\mathrm{N}}(r)2\pi\mu r. \tag{13}$$

where r_2 represents the distance from the typical user to its nearest LOS BS. Therefore, the minimum distance r_2 between the typical user and the LOS BSs can be computed by

$$r_2 = r\omega^{-\frac{E[K_i]}{\alpha}}. \tag{14}$$

Proof: See Appendix B. ∎

Due to the attenuation of interior walls, the path loss of an NLOS link is generally smaller than that of an LOS link with the same link length. Therefore, the calculation of (13) should be discussed by the numerical relationship among r, r_2 and the possible maximum link length D.

If the length range of the NLOS serving link r is $(0, r_D]$, the length range of NLOS interferences would accordingly be $[r, r_D]$ and the length range of LOS interferences would accordingly be $[r_2, D)$. Specifically, the value of r_D is delimited by D and r_2, where the possible maximum length of LOS links is D. Within the the length range of the NLOS serving link, the LOS and NLOS interferences both exist. Substituting (5) and (6) into (13), the PDF of the typical user connecting to the nearest NLOS BS at distance r, where its range is within $(0, r_D]$, is rewritten as

$$\begin{aligned}\hat{f}_{\mathrm{N}}(r)^a &= \{\hat{f}_{\mathrm{N}}(r) \,|\, 0 < r \le r_D\} \\ &= e^{-\int_0^{r_2} P_{\mathrm{L}}(r)2\pi\mu t\mathrm{d}t} \times e^{-\int_0^{r} P_{\mathrm{N}}(r)2\pi\mu t\mathrm{d}t} \times P_{\mathrm{N}}(r)2\pi\mu r \\ &= 2\pi\mu r(1-e^{-\beta r}) \times e^{-2\pi\mu(\frac{r^2}{2}+\frac{e^{-\beta r}(1+\beta r)-1}{\beta^2})} \\ &\quad \times e^{-2\pi\mu(\frac{1-e^{-\beta r_2}(1+\beta r_2)}{\beta^2})}.\end{aligned} \tag{15}$$

If the length range of the NLOS serving link r is (r_D, D), the length range of NLOS interferences would accordingly be $[r, D)$ and the possible minimum length of the LOS links r_2 exceeds the boundary of indoor area. Consequently, only the NLOS interference exists. Substituting (6) into (13), the PDF of the typical user connecting to nearest NLOS BS at distance r, where its range is within (r_D, D), is rewritten as

$$\begin{aligned}\hat{f}_{\mathrm{N}}(r)^b &= \{\hat{f}_{\mathrm{N}}(r) \,|\, r_D < r < D\} \\ &= e^{-\int_0^{r} P_{\mathrm{N}}(r)2\pi\mu t\mathrm{d}t} \times P_{\mathrm{N}}(r)2\pi\mu r \\ &= 2\pi\mu r(1-e^{-\beta r}) \times e^{-2\pi\mu(\frac{r^2}{2}+\frac{e^{-\beta r}(1+\beta r)-1}{\beta^2})}.\end{aligned} \tag{16}$$

B. Downlink Coverage Probability

In this subsection, the conditional coverage probabilities are derived with the strongest received signal UAS, when the typical user is connected to an LOS BS or NLOS BS, respectively.

Theorem 1. *The conditional coverage probability of the typical user, when it is connected to an LOS BS, is computed by*

$$\begin{aligned}&\mathbb{P}\left\{\frac{p_T h_j L_{\mathrm{R}}(d_{\mathrm{LOS}_j})}{I_{\mathrm{L}}+I_{\mathrm{N}}+N_0} > T | d_{\mathrm{LOS}_j} = r, 0 < r < D\right\} \\ =&\exp\left(-2\pi\mu\left[\int_r^D e^{-\beta t}\left[1-\frac{t^\alpha}{t^\alpha+Tr^\alpha}\right]t\mathrm{d}t \quad + \right.\right. \\ &\left.\left.\int_{r_1}^D (1-e^{-\beta t})\left[1-\frac{t^\alpha}{t^\alpha+Tr^\alpha\omega^{\beta t}}\right]t\mathrm{d}t\right]\right)\times\exp(-\frac{N_0}{p_T\eta_0}Tr^\alpha).\end{aligned} \tag{17}$$

Proof: See Appendix C. ∎

Based on (12) and (17), the unconditional coverage probability of the LOS serving link with smallest path loss is computed by

$$P_c^{\mathrm{L}}(T) = \int_0^D \left\{\mathbb{P}\left[\frac{p_T h_j L_{\mathrm{R}}(d_{\mathrm{LOS}_j})}{I_{\mathrm{L}}+I_{\mathrm{N}}+N_0} > T\right]\hat{f}_{\mathrm{L}}(r)\,\middle|\, 0 < r < D\right\}\mathrm{d}r. \tag{18}$$

When the typical user is associated with an NLOS BS, the conditional coverage probability is influenced by the numerical relationship among r, r_2 and the maximum link length D in an indoor area. According to the discussion of NLOS cases in Section III-A, the range of serving link length is divided into $(0, r_D]$ and (r_D, D), where r_D can be derived by the relationship between r_2 and D.

Theorem 2. *According to the discussion of r in the NLOS case, the coverage probability conditioned on the length range of the serving NLOS link is $(0, r_D]$, where both the LOS and NLOS interferences exist, is given by*

$$\begin{aligned}&\mathbb{P}\left\{\frac{p_T h_j L_{\mathrm{R}}(d_{\mathrm{NLOS}_j})}{I_{\mathrm{L}}+I_{\mathrm{N}}+N_0} > T | d_{\mathrm{NLOS}_j} = r, 0 < r \le r_D\right\} \\ =&\exp\left(-2\pi\mu\left[\int_{r_2}^D e^{-\beta t}\left[1-\frac{t^\alpha}{t^\alpha+Tr^\alpha\omega^{-\beta r}}\right]t\mathrm{d}t \quad + \right.\right. \\ &\left.\left.\int_r^{r_D}(1-e^{-\beta t})\left[1-\frac{t^\alpha}{t^\alpha+Tr^\alpha\omega^{\beta(t-r)}}\right]t\mathrm{d}t\right]\right) \\ \times&\quad \exp(-\frac{N_0}{p_T\eta_0}Tr^\alpha\omega^{-\beta r}).\end{aligned} \tag{19}$$

Conditioned on the length range of the serving NLOS link being (r_D, D), the coverage probability, where the interferences only come from the NLOS links, is given by

$$\mathbb{P}\left\{\frac{p_T h_j L_{\mathrm{R}}(d_{\mathrm{NLOS}_j})}{I_{\mathrm{N}}+N_0} > T | d_{\mathrm{NLOS}_j} = r, r_D < r < D\right\}$$
$$= \exp\left(-2\pi\mu\left[\int_r^D (1-e^{-\beta t})\left[1-\frac{t^\alpha}{t^\alpha + Tr^\alpha \omega^{\beta(t-r)}}\right] t\mathrm{d}t\right]\right)$$
$$\times \quad \exp\left(-\frac{N_0}{p_T \eta_0} T r^\alpha \omega^{-\beta r}\right). \tag{20}$$

Proof: See Appendix D. ∎

Therefore, the unconditional coverage probability $P_c^{\mathrm{N}}(T)$ of the NLOS serving link with the smallest path loss is computed by combining (15), (16), (19) and (20) as

$$P_c^{\mathrm{N}}(T)$$
$$= \int_0^{r_D} \left\{\mathbb{P}\left[\frac{p_T h_j L_{\mathrm{R}}(d_{\mathrm{NLOS}_j})}{I_{\mathrm{L}}+I_{\mathrm{N}}+N_0} > T\right] \hat{f}_{\mathrm{N}}(r)^a \middle| 0 < r \le r_D\right\} \mathrm{d}r$$
$$+ \int_{r_D}^{D} \left\{\mathbb{P}\left[\frac{p_T h_j L_{\mathrm{R}}(d_{\mathrm{NLOS}_j})}{I_{\mathrm{N}}+N_0} > T\right] \hat{f}_{\mathrm{N}}(r)^b \middle| r_D < r < D\right\} \mathrm{d}r. \tag{21}$$

The Stochastic geometry-based framework for indoor SCNs of coverage probability under the smallest path-loss UAS is completed by plugging the LOS BS-UE connection part of coverage probability (18) and the NLOS BS-UE connection part of coverage probability (21) into (9).

IV. Numerical Evaluation

In this section, the numerical results based on the analytical expressions in Section III are presented with different wall attenuations and validated by Monte Carlo simulations. The numerical results are computed using the analytical expression in (9). The Monte-Carlo simulation results include three typical layouts of walls (random layout, binary orientation layout and Manhattan grid). Each simulation result is obtained based on 10^5 independent random realisations of indoor SCN scenarios including the floor plans, distributions of BSs and interior walls and channel model. Both numerical evaluation and Monte Carlo simulations are performed using MATLAB. The default simulation parameter values are listed in Table I [2]. Besides, we futher analyse the performance of SCNs with different wall attenuations for various densities of BSs and walls.

Fig. 2 shows, under random layout of interior walls, the analytical and simulation results of coverage probability with different wall attenuations. The curves present the coverage probabilities of the nearest LOS UAS (18), the nearest NLOS UAS (21), and the strongest received signal UAS (9), respectively. It is observed that the curves of the analytical results generally match those of the Monte Carlo simulations well, but with a minor gap between them. The deviations between analytical and simulation results are caused by replacing the factor of ω^{K_i} with $\omega^{E[K_i]}$ in the derived expression of coverage probability. Based on the curves with two different values of wall attenuations (3 and 10 dB) shown in Fig. 2, it can be seen that a larger value of wall attenuation leads to a higher coverage probability, as larger wall attenuation reduces the inter-cell interference.

TABLE I
Parameters for Numerical Simulations

Parameter	Value
Maximum link length	20 m
Transmit power	$p_T = 24$ dBm
Noise power	$N_0 = -95$ dBm
Path loss at reference distance	$\eta_0 = -38.5$ dB
BS density	$\mu = 0.01$ m^{-2}
Average width of walls	$L = 3$ m
Wall density	Random and binary orientation layout: $\lambda = 0.05$ m^{-2} Manhattan grid: $\lambda' = \frac{\lambda L}{2} = \frac{3}{40}$ m^{-2}
Wall Orientation	Random layout: $\psi_k \in [0, \pi)$ Binary orientation layout: $\psi_k \in \{0, \frac{\pi}{2}\}$
Path-loss exponent	$\alpha = 2$

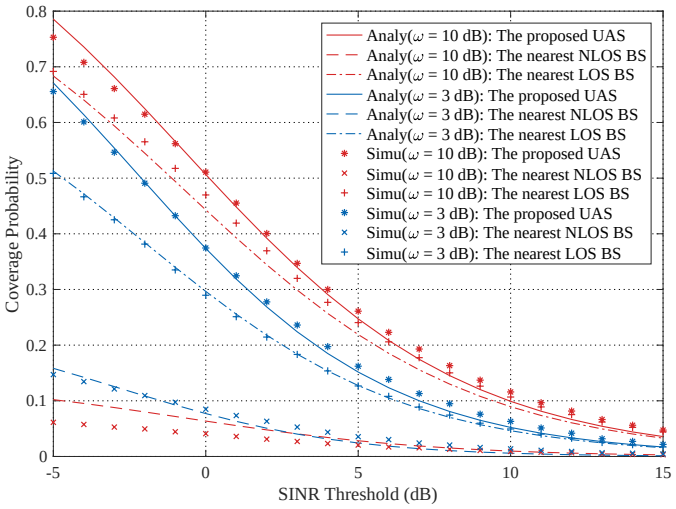

Fig. 2. The analytical and simulation results under random layout. The analytical coverage probability for the strongest received signal LOS BS serving case , the strongest received signal NLOS BS serving case and the strongest received signal case UAS is calculated using (18), (21) and (9), respectively.

Fig. 3 compares the coverage probabilities under different wall layouts. It is worth mentioning that the difference between random layout and binary orientation layout is neglectable. This reveals that the wall orientation has limited influence on the performance of our proposed SCN model. Comparing the simulation results of Manhattan grid with other wall layouts, we can see that these three wall layouts with the same average wall volume result in similar network performance in terms of the coverage probability. Since Manhattan grid model is a good approximation of practical wall layout [20], our analytical expression of the coverage probability can serve as a tight lower bound of the practical indoor wireless coverage performance.

Fig. 4 illustrates the analytical results of the coverage

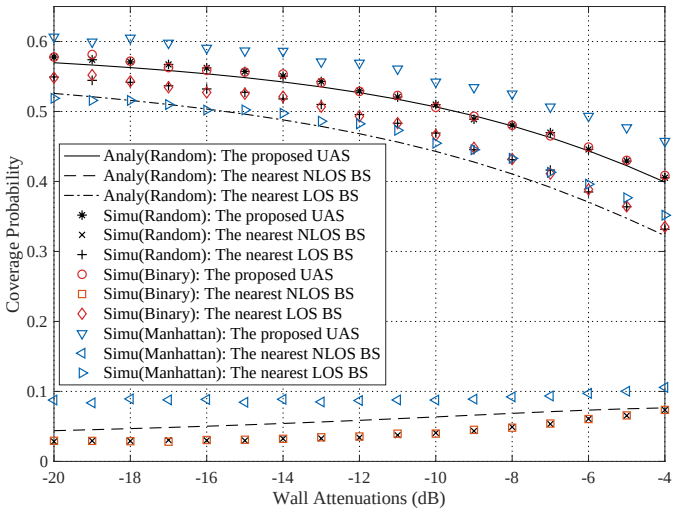

Fig. 3. The analytical results under the random layout and simulation results under the random layout, binary orientation layout and Manhattan grid, for the SINR threshold $T = 0\,\mathrm{dB}$.

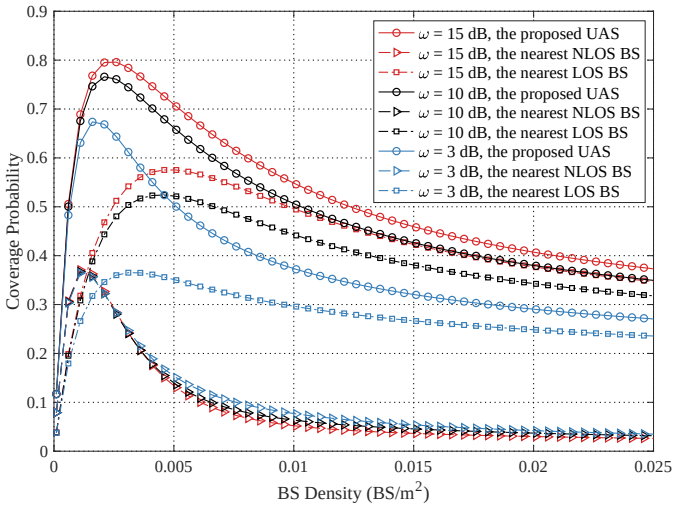

Fig. 4. The analytical results of coverage probability versus the BS density under the random layout for wall attenuations of 3, 10 and 15 dB and the SINR threshold $T = 0\,\mathrm{dB}$.

probability with different BS densities and wall attenuations (3, 10 and 15 dB). From the analytical curves, it is found that the coverage probability of the nearest NLOS UAS first rapidly grows to the maximum with the increase of BS density, then declines quickly. Relatively, the variation of the nearest NLOS UAS is smoother. It can be seen that the serving BS is mainly in NLOS conditions when BS density is low, and the LOS BS becomes the dominant serving BS with adequate BSs. An apparent observation is that there is an optimal BS density maximizing the coverage probability. The optimal BS density increases with the increase of the wall attenuation. Besides, the curves of coverage probability flatten after the sufficiently high density of BS. From the curves of four different wall attenuations in Fig. 4, it can be concluded that larger wall attenuations lead to larger coverage probability under the dense SCNs.

Fig. 5 shows the analytical results of the coverage proba-

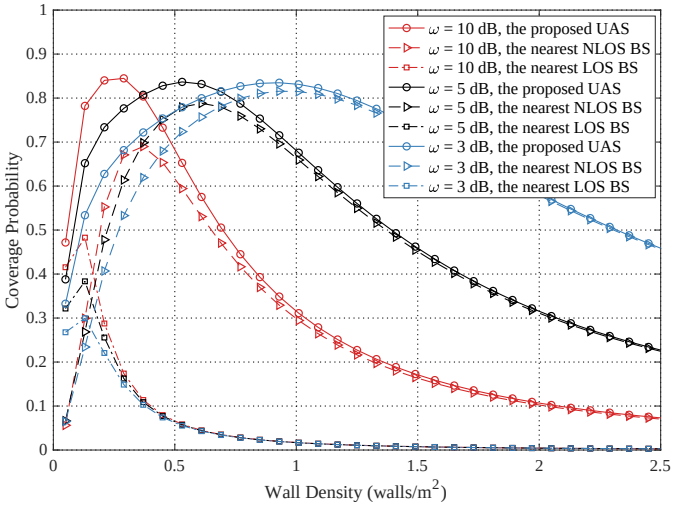

Fig. 5. The analytical results of coverage probability versus the wall density under the random layout for wall attenuations of 3, 5 and 10 dB and the SINR threshold $T = 0\,\mathrm{dB}$.

bility with different wall densities and wall attenuations (3, 5 and 10 dB). It can be observed that the coverage probability of the nearest NLOS BS UAS case first increases with the wall density and then sharply drops after the turning point. This is because appropriate number of walls reduce inter-cell interference, thereby improving the coverage probability. With further increase of the wall density, the power of both serving and interfering links decreases. Then, the coverage probability gradually descends and is mainly effected by the AWGN power since the power of the serving link is of the same magnitude as AWGN power. Moreover, we observe that the critical wall density, i.e., the wall density that maximizes the coverage probability, decreases with the increase of the wall attenuation.

V. Conclusion

In this paper, we have proposed a distance-dependent indoor channel model that distinguishes LOS and NOLS links and includes the effects of interior wall attenuation. Based on the proposed channel model, we have derived the downlink coverage probability of an indoor SCN under the strongest received signal UAS. The analytical results show a good fit with Monte Carlo simulations. Besides, the simulation results reveal that for the same average volume of interior walls, the downlink coverage probability of the indoor SCN is similar under the three different layouts of interior walls, i.e., random layout, binary orientation layout, and Manhattan grid. From the analytical results, it can be observed that the coverage probability is sensitive to the BS density for low-to-medium BS densities, and there exists an optimal BS density that maximises the coverage probability. For a given BS density, the coverage probability first increases with the wall density, as a larger wall density leads to less inter-cell interference. After reaching a peak, the coverage probability starts to decrease since the SCN becomes noise-limited when the wall density is very high.

In this paper, we focus on the coverage performance analysis of the SCN on a single floor. In our future work, we will investigate the effects of interior walls and ceilings on the coverage performance of the SCN in a 3D multi-story building. We will extend the proposed indoor SCN model to the analysis of indoor millimeter-wave/terahertz networks. Moreover, the effect of interference mitigation techniques, e.g., multi-antenna transmission will be investigated.

Appendix A
Proof of Lemma 1

If the strongest received signal link is LOS, the event E_1 can be defined as E_1 ={The nearest BS located at the distance r has an LOS path to the typical user}. According to [8], the cumulative distribution function (CDF) of event E_1 is

$$F_{\mathrm{L}}(r) = 1 - e^{-\int_0^r P_{\mathrm{L}} 2\pi\mu t \mathrm{d}t}, \tag{22}$$

and the PDF of event E_1 is the derivative of CDF, derived as

$$f_{\mathrm{L}}(r) = e^{-\int_0^r P_{\mathrm{L}} 2\pi\mu t \mathrm{d}t} \times P_{\mathrm{L}} 2\pi\mu r. \tag{23}$$

Furthermore, the event E_2 is defined as E_2 ={the typical user is associated with a BS at distance d_{LOS_j}}. Specifically, the serving BS is assumed as the closest LOS BS to the typical user, the event E_2 is conditioned on event E_1: $d_{\mathrm{LOS}_j} = r$. This assumption means there is no NLOS BSs outperforming the LOS BSs within distance r. According to [8], the probability of E_2 conditioned on $d_{\mathrm{LOS}_j} = r$ can be computed by

$$\mathbb{P}[E_2 | d_{\mathrm{LOS}_j} = r] = e^{-\int_0^{r_1} P_{\mathrm{N}} 2\pi\mu r \mathrm{d}r}. \tag{24}$$

Denoting C^{L} as the distance between the typical user and its serving LOS BS, the CDF of C^{L} can be derived as

$$\begin{aligned}
\overline{F}_{d_{\mathrm{LOS}_j}}(r) &= \mathbb{P}[C^{\mathrm{L}} > r] \\
&= \int_0^D \mathbb{P}[C^{\mathrm{L}} > r | d_{\mathrm{LOS}_j} = x] f_{\mathrm{L}}(x) \mathrm{d}x \\
&\overset{(a)}{=} \int_0^r 0 \times f_{\mathrm{L}}(x) \mathrm{d}x \quad + \\
&\quad \int_r^D \mathbb{P}[E_2 | d_{\mathrm{LOS}_j} = x] f_{\mathrm{L}}(x) \mathrm{d}x \\
&= \int_r^D \mathbb{P}[E_2 | d_{\mathrm{LOS}_j} = x] f_{\mathrm{L}}(x) \mathrm{d}x,
\end{aligned} \tag{25}$$

in step (a), when $x \in (0, r]$, $\mathbb{P}[C^{\mathrm{L}} > r | d_{\mathrm{LOS}_j} = x] = 0$; when $x \in (r, D)$, $\mathbb{P}[C^{\mathrm{L}} > r | d_{\mathrm{LOS}_j} = x]$ equals to the probability of conditional event E_2, i.e., $\mathbb{P}[C^{\mathrm{L}} > r | d_{\mathrm{LOS}_j} = x] = \mathbb{P}[E_2 | d_{\mathrm{LOS}_j} = x]$.

Thus, in (12), PDF of d_{LOS_j}, can be derived by the derivative of (25).

Appendix B
Proof of Lemma 2

For the strongest received signal NLOS connectivity, the event E_3 is defined as E_3 ={The nearest BS located at the distance r has an NLOS path to the typical user}. Similar to (23), the PDF of event E_3 is obtained as

$$f_{\mathrm{N}}(r) = e^{-\int_0^r P_{\mathrm{N}} 2\pi\mu t \mathrm{d}t} \times P_{\mathrm{N}} 2\pi\mu r. \tag{26}$$

The event E_4 is defined as E_4 ={the typical user is associated with a BS at distance d_{NLOS_j}, where $d_{NLOS_j} = r$}, which means the typical user is served by the closest NLOS BS, i.e., the path-loss function of an LOS link $L_{\mathrm{R}}(d_{LOS_i})$ is always smaller than the path-loss function of the NLOS serving link $L_{\mathrm{R}}(r)$.

Then, the probability of event E_4 conditioned on $d_{NLOS_j} = r$ can be derived as

$$\mathbb{P}[E_4 | d_{\mathrm{NLOS}_j} = r] = e^{-\int_0^{r_2} P_{\mathrm{L}} 2\pi\mu t \mathrm{d}t}. \tag{27}$$

Denoting C^{N} as the distance between the typical user and its serving NLOS BS, the CDF of C^{N} can be derived as

$$\begin{aligned}
\overline{F}_{d_{\mathrm{NLOS}_j}}(r) &= \mathbb{P}[C^{\mathrm{N}} > r] \\
&= \int_0^D \mathbb{P}[C^{\mathrm{N}} > r | d_{\mathrm{NLOS}_j} = x] f_{\mathrm{N}}(x) \mathrm{d}x \\
&\overset{(a)}{=} \int_0^r 0 \times f_{\mathrm{N}}(x) \mathrm{d}x \quad + \\
&\quad \int_r^D \mathbb{P}[E_4 | d_{\mathrm{NLOS}_j} = x] f_{\mathrm{N}}(x) \mathrm{d}x \\
&= \int_r^D \mathbb{P}[E_4 | d_{\mathrm{NLOS}_j} = x] f_{\mathrm{N}}(x) \mathrm{d}x,
\end{aligned} \tag{28}$$

in step (a), when $x \in (0, r]$, $\mathbb{P}[C^{\mathrm{N}} > r | d_{\mathrm{NLOS}_j} = x] = 0$; when $x \in (r, D)$, $\mathbb{P}[C^{\mathrm{N}} > r | d_{\mathrm{NLOS}_j} = x]$ equals to the probability of conditional event E_2, i.e., $\mathbb{P}[C^{\mathrm{N}} > r | d_{\mathrm{NLOS}_j} = x] = \mathbb{P}[E_2 | d_{\mathrm{NLOS}_j} = x]$.

Therefore, the (13) can be derived by the derivative of the (28).

Appendix C
Proof of Theorem 1

For the cases of LOS serving links, substituting (1) and (5)-(8) into (9), the conditional coverage probability is computed by

$$\begin{aligned}
&\mathbb{P}\left\{ \frac{p_T h_j L_{\mathrm{R}}(d_{\mathrm{LOS}_j})}{I_{\mathrm{L}} + I_{\mathrm{N}} + N_0} > T | d_{\mathrm{LOS}_j} = r, 0 < r < D \right\} \\
=&\mathbb{P}\Bigg\{ h_j > \Bigg(\sum_{m \in \Phi_{\mathrm{L}}/j, d_m \in [r, D)} p_T h_m L_{\mathrm{R}}(d_m) \quad + \\
&\sum_{n \in \Phi_{\mathrm{N}}, d_n \in [r_1, D)} p_T h_n L_{\mathrm{R}}(d_n) + N_0 \Bigg) \frac{T}{p_T} L_{\mathrm{R}}(d_j)^{-1} \Bigg\} \\
=&\mathbb{E}\Bigg[\exp\Bigg(- \Bigg(\sum_{m \in \Phi_{\mathrm{L}}/j, d_m \in [r, D)} h_m L_{\mathrm{R}}(d_m) \quad + \\
&\sum_{n \in \Phi_{\mathrm{N}}, d_n \in [r_1, D)} h_n L_{\mathrm{R}}(d_n) + \frac{N_0}{p_T} \Bigg) T L_{\mathrm{R}}(d_j)^{-1} \Bigg) \Bigg] \\
=&\mathbb{E}\Bigg[\prod_{m \in \Phi_{\mathrm{L}}/j, d_m \in [r, D)} \mathbb{E}_{h_m} \left[\exp\left(-h_m d_m^{-\alpha} T r^{\alpha} \right) \right] \quad \times \\
&\prod_{n \in \Phi_{\mathrm{N}}, d_n \in [r_1, D)} \mathbb{E}_{h_n} \Big[\exp\Big(-h_n d_n^{-\alpha} T r^{\alpha} \omega^{E[K_n]} \Big) \Big] \times \exp\Big(-\frac{N_0}{p_T \eta_0} T r^{\alpha} \Big) \Bigg]
\end{aligned}$$

$$
\begin{aligned}
=&\mathbb{E}\left[\prod_{m\in\Phi_{\mathrm{L}}/j,d_m\in[r,D)}\frac{d_m^{\alpha}}{d_m^{\alpha}+Tr^{\alpha}}\right]\quad\times\\
&\mathbb{E}\left[\prod_{n\in\Phi_{\mathrm{N}},d_n\in[r_1,D)}\frac{d_n^{\alpha}}{d_n^{\alpha}+Tr^{\alpha}\omega^{E[K_n]}}\right]\times\exp(-\frac{N_0}{p_T\eta_0}Tr^{\alpha})\\
\overset{(a)}{=}&\exp\Bigg(-2\pi\left[\int_r^D\mu P_{\mathrm{L}(m)}\left[1-\frac{t^{\alpha}}{t^{\alpha}+Tr^{\alpha}}\right]\mathrm{t}\mathrm{d}t\quad+\right.\\
&\left.\int_{r_1}^D\mu P_{\mathrm{N}(n)}\left[1-\frac{t^{\alpha}}{t^{\alpha}+Tr^{\alpha}\omega^{\beta t}}\right]\mathrm{t}\mathrm{d}t\right]\Bigg)\times\exp(-\frac{N_0}{p_T\eta_0}Tr^{\alpha})\\
=&\exp\Bigg(-2\pi\mu\left[\int_r^D e^{-\beta t}\left[1-\frac{t^{\alpha}}{t^{\alpha}+Tr^{\alpha}}\right]\mathrm{t}\mathrm{d}t\quad+\right.\\
&\left.\int_{r_1}^D(1-e^{-\beta t})\left[1-\frac{t^{\alpha}}{t^{\alpha}+Tr^{\alpha}\omega^{\beta t}}\right]\mathrm{t}\mathrm{d}t\right]\Bigg)\times\exp(-\frac{N_0}{p_T\eta_0}Tr^{\alpha}),
\end{aligned}
\tag{29}
$$

where step (a) is obtained using the probability generating functional (PGF) of PPP for the LOS and NLOS transmitters. In Addition, the densities of LOS and NLOS transmitters in the PGFL process are calculated by incorporating the probability of LOS and NLOS links with the BS density μ, respectively.

Appendix D
Proof of Theorem 2

According to the discussion of r in the NLOS case, the coverage probability conditioned on the length range of the serving NLOS link is $(0, r_D]$, where both the LOS and NLOS interferences exist, is given by

$$
\begin{aligned}
&\mathbb{P}\left\{\frac{p_T h_j L_{\mathrm{R}}(d_{\mathrm{NLOS}_j})}{I_{\mathrm{L}}+I_{\mathrm{N}}+N_0}>T|d_{\mathrm{NLOS}_j}=r,0<r\le r_D\right\}\\
=&\mathbb{P}\Bigg\{h_j>\Bigg(\sum_{m\in\Phi_{\mathrm{L}},d_m\in[r_2,D)}p_T h_m L_{\mathrm{R}}(d_m)\quad+\\
&\sum_{n\in\Phi_{\mathrm{N}}/j,d_n\in[r,r_D]}p_T h_n L_{\mathrm{R}}(d_n)+N_0\Bigg)\frac{T}{p_T}L_{\mathrm{R}}(d_j)^{-1}\Bigg\}\\
=&\mathbb{E}\Bigg[\exp\Bigg(-\Bigg(\sum_{m\in\Phi_{\mathrm{L}},d_m\in(r_2,D)}h_m L_{\mathrm{R}}(d_m)\quad+\\
&\sum_{n\in\Phi_{\mathrm{N}}/j,d_n\in[r,r_D]}h_n L_{\mathrm{R}}(d_n)+\frac{N_0}{p_T}\Bigg)TL_{\mathrm{R}}(d_j)^{-1}\Bigg)\Bigg]\\
=&\mathbb{E}\Bigg[\prod_{m\in\Phi_{\mathrm{L}},d_m\in[r_2,D)}\mathbb{E}_{h_m}\left[\exp\left(-h_m d_m^{-\alpha}Tr^{\alpha}\omega^{-E[K_j]}\right)\right]\times\\
&\prod_{n\in\Phi_{\mathrm{N}}/j,d_n\in[r,r_D]}\mathbb{E}_{h_n}\left[\exp\left(-h_n d_n^{-\alpha}Tr^{\alpha}\omega^{-E[K_j]}\omega^{E[K_n]}\right)\right]\\
&\times\quad\exp(-\frac{N_0}{p_T\eta_0}Tr^{\alpha}\omega^{-E[K_j]})\Bigg]\\
=&\mathbb{E}\left[\prod_{m\in\Phi_{\mathrm{L}},d_m\in[r_2,D)}\frac{d_m^{\alpha}}{d_m^{\alpha}+Tr^{\alpha}\omega^{-E[K_j]}}\right]\quad\times\\
&\mathbb{E}\left[\prod_{n\in\Phi_{\mathrm{N}}/j,d_n\in[r,r_D]}\frac{d_n^{\alpha}}{d_n^{\alpha}+Tr^{\alpha}\omega^{-E[K_j]}\omega^{E[K_n]}}\right]\\
&\times\quad\exp(-\frac{N_0}{p_T\eta_0}Tr^{\alpha}\omega^{-E[K_j]})\\
\overset{(a)}{=}&\exp\Bigg(-2\pi\left[\int_{r_2}^D\mu P_{\mathrm{L}(m)}\left[1-\frac{t^{\alpha}}{t^{\alpha}+Tr^{\alpha}\omega^{-\beta r}}\right]\mathrm{t}\mathrm{d}t\quad+\right.\\
&\left.\int_r^{r_D}\mu P_{\mathrm{N}(n)}\left[1-\frac{t^{\alpha}}{t^{\alpha}+Tr^{\alpha}\omega^{\beta(t-r)}}\right]\mathrm{t}\mathrm{d}t\right]\Bigg)\\
&\times\quad\exp(-\frac{N_0}{p_T\eta_0}Tr^{\alpha}\omega^{-\beta r})\\
=&\exp\Bigg(-2\pi\mu\left[\int_{r_2}^D e^{-\beta t}\left[1-\frac{t^{\alpha}}{t^{\alpha}+Tr^{\alpha}\omega^{-\beta r}}\right]\mathrm{t}\mathrm{d}t\quad+\right.\\
&\left.\int_r^{r_D}(1-e^{-\beta t})\left[1-\frac{t^{\alpha}}{t^{\alpha}+Tr^{\alpha}\omega^{\beta(t-r)}}\right]\mathrm{t}\mathrm{d}t\right]\Bigg)\\
&\times\quad\exp(-\frac{N_0}{p_T\eta_0}Tr^{\alpha}\omega^{-\beta r}),
\end{aligned}
\tag{30}
$$

where step (a) is obtained using the PGF of PPP for the LOS and NLOS transmitters.

Besides, the coverage probability conditioned on the length range of the serving NLOS link is (r_D, D), where the interference only comes from the NLOS links, is given by

$$
\begin{aligned}
&\mathbb{P}\left\{\frac{p_T h_j L_{\mathrm{R}}(d_{\mathrm{NLOS}_j})}{I_{\mathrm{N}}+N_0}>T|d_{\mathrm{NLOS}_j}=r,r_D<r<D\right\}\\
=&\mathbb{P}\Bigg\{h_j>\Bigg(\sum_{n\in\Phi_{\mathrm{N}}/j,d_n\in(r_D,D)}p_T h_n S_n d_n^{-\alpha}+N_0\Bigg)\frac{T}{p_T}L_{\mathrm{R}}(d_j)^{-1}\Bigg\}\\
=&\mathbb{E}\left[\exp\left(-\left(\sum_{n\in\Phi_{\mathrm{N}}/j,d_n\in(r_D,D)}h_n S_n d_n^{-\alpha}+\frac{N_0}{p_T}\right)TL_{\mathrm{R}}(d_j)^{-1}\right)\right]\\
=&\mathbb{E}\Bigg[\prod_{n\in\Phi_{\mathrm{N}}/j,d_n\in(r_D,D)}\mathbb{E}_{h_n}\left[\exp\left(-h_n d_n^{-\alpha}Tr^{\alpha}\omega^{-E[K_j]}\omega^{E[K_n]}\right)\right]\\
&\times\quad\exp(-\frac{N_0}{p_T\eta_0}Tr^{\alpha}\omega^{-E[K_j]})\Bigg]\\
=&\mathbb{E}\left[\prod_{n\in\Phi_{\mathrm{N}}/j,d_n\in(r_D,D)}\frac{d_n^{\alpha}}{d_n^{\alpha}+Tr^{\alpha}\omega^{-E[K_j]}\omega^{E[K_n]}}\right]\\
&\times\quad\exp(-\frac{N_0}{p_T\eta_0}Tr^{\alpha}\omega^{-E[K_j]})\\
\overset{(a)}{=}&\exp\left(-2\pi\left[\int_r^D\mu P_{\mathrm{N}(n)}\left[1-\frac{t^{\alpha}}{t^{\alpha}+Tr^{\alpha}\omega^{\beta(t-r)}}\right]\mathrm{t}\mathrm{d}t\right]\right)\\
&\times\quad\exp(-\frac{N_0}{p_T\eta_0}Tr^{\alpha}\omega^{-\beta r})\\
=&\exp\left(-2\pi\mu\left[\int_r^D(1-e^{-\beta t})\left[1-\frac{t^{\alpha}}{t^{\alpha}+Tr^{\alpha}\omega^{\beta(t-r)}}\right]\mathrm{t}\mathrm{d}t\right]\right)\\
&\times\quad\exp(-\frac{N_0}{p_T\eta_0}Tr^{\alpha}\omega^{-\beta r}),
\end{aligned}
\tag{31}
$$

where step (a) is the PGF of PPP for the NLOS transmitters.

REFERENCES

[1] T. Barnett, S. Jain, U. Andra, and T. Khurana, "Cisco visual networking index (vni) complete forecast update, 2017–2022," *Americas/EMEAR CKN Presentation*, 2018.

[2] C. Chen, Y. Zhang, J. Zhang, X. Chu, and J. Zhang, "On the performance of indoor multi-story small-cell networks," *IEEE Trans. Wireless Commun.*, vol. 20, no. 2, pp. 1336–1348, Feb. 2021.

[3] T. Nakamura, S. Nagata, A. Benjebbour, Y. Kishiyama, T. Hai, S. Xiaodong, Y. Ning, and L. Nan, "Trends in small cell enhancements in lte advanced," *IEEE Commun. Mag.*, vol. 51, no. 2, pp. 98–105, 2013.

[4] J. Liu, T. Kou, Q. Chen, and H. D. Sherali, "Femtocell base station deployment in commercial buildings: A global optimization approach," *IEEE J. Sel. Areas Commun.*, vol. 30, no. 3, pp. 652–663, 2012.

[5] W. Yang, J. Zhang, A. A. Glazunov, and J. Zhang, "Line-of-sight probability for channel modeling in 3-d indoor environments," *IEEE Antennas Wirel. Propag. Lett.*, vol. 19, no. 7, pp. 1182–1186, 2020.

[6] H. Zheng, J. Zhang, H. Li, Q. Hong, H. Hu, and J. Zhang, "Exact line-of-sight probability for channel modeling in typical indoor environments," *IEEE Antennas Wirel. Propag. Lett*, vol. 17, no. 7, pp. 1359–1362, 2018.

[7] Y. Zhang, C. Chen, S. Yang, J. Zhang, X. Chu, and J. Zhang, "How friendly are building materials as reflectors to indoor los mimo communications?," *IEEE Internet Things J.*, vol. 7, no. 9, pp. 9116–9127, 2020.

[8] J. G. Andrews, F. Baccelli, and R. K. Ganti, "A tractable approach to coverage and rate in cellular networks," *IEEE Trans. Wireless Commun.*, vol. 59, no. 11, pp. 3122–3134, Nov. 2011.

[9] H. S. Dhillon, R. K. Ganti, F. Baccelli, and J. G. Andrews, "Modeling and analysis of k-tier downlink heterogeneous cellular networks," *IEEE J.Sel.Areas Commun.*, vol. 30, no. 3, pp. 550–560, 2012.

[10] H.-S. Jo, Y. J. Sang, P. Xia, and J. G. Andrews, "Heterogeneous cellular networks with flexible cell association: A comprehensive downlink sinr analysis," *IEEE Trans. Wireless Commun.*, vol. 11, no. 10, pp. 3484–3495, 2012.

[11] T. Bai, R. Vaze, and R. W. Heath, "Analysis of blockage effects on urban cellular networks," *IEEE Trans. Wireless Commun.*, vol. 13, no. 9, pp. 5070–5083, Spet. 2014.

[12] M. Ding, P. Wang, D. Lpez-Prez, G. Mao, and Z. Lin, "Performance impact of LoS and NLoS transmissions in dense cellular networks," *IEEE Trans. Wireless Commun.*, vol. 15, no. 3, pp. 2365–2380, Mar. 2016.

[13] I. Atzeni, J. Arnau, and M. Kountouris, "Downlink cellular network analysis with los/nlos propagation and elevated base stations," *IEEE Trans. Wireless Commun.*, vol. 17, no. 1, pp. 142–156, 2018.

[14] C. Chen, J. Zhang, X. Chu, and J. Zhang, "On the deployment of small cells in 3d hetnets with multi-antenna base stations," *IEEE Trans. Wireless Commun.*, vol. 21, no. 11, pp. 9761–9774, 2022.

[15] T. Bai and R. W. Heath, "Coverage and Rate Analysis for Millimeter-Wave Cellular Networks," *IEEE Trans. Wireless Commun.*, vol. 14, no. 2, pp. 1100–1114, Feb. 2015.

[16] M. Di Renzo, "Stochastic geometry modeling and analysis of multi-tier millimeter wave cellular networks," *IEEE Trans. Wireless Commun.*, vol. 14, no. 9, pp. 5038–5057, 2015.

[17] C. Chen, J. Zhang, X. Chu, and J. Zhang, "On the optimal base-station height in mmwave small-cell networks considering cylindrical blockage effects," *IEEE Trans. Veh. Technol.*, vol. 70, no. 9, pp. 9588–9592, 2021.

[18] J. Lee, X. Zhang, and F. Baccelli, "A 3-D spatial model for in-building wireless networks with correlated shadowing," *IEEE Trans. Wireless Commun.*, vol. 15, no. 11, pp. 7778–7793, Nov. 2016.

[19] L. Zhang, X. Gu, Z. Liu, L. Zhang, and H. Moon, "Modeling and analysis of indoor coverage probability for future 3d dense mobile networks," in *WPMC*, pp. 247–252, 2017.

[20] M. K. Muller, M. Taranetz, and M. Rupp, "Analyzing wireless indoor communications by blockage models," *IEEE Access*, vol. 5, pp. 2172–2186, 2017.

[21] M. K. Mller, M. Taranetz, and M. Rupp, "Effects of wall-angle distributions in indoor wireless communications," in *SPAWC*, pp. 1–5, 2016.

[22] H. Zheng, J. Zhang, H. Hu, and J. Zhang, "The analysis of indoor wireless communications by a blockage model in ultra-dense networks," in *IEEE VTC-Fall*, pp. 1–6, 2018.

[23] Z. Li, H. Hu, J. Zhang, and J. Zhang, "Impact of wall penetration loss on indoor wireless networks," *IEEE Antennas Wirel. Propag. Lett.*, vol. 20, no. 10, pp. 1888–1892, 2021.

[24] Y. Wang, H. Zheng, and X. Chu, "Impact of wall blockage on los user association strategy in indoor small cell networks," in *IEEE ISAP*, pp. 579–580, 2020.

[25] Y. Wang, H. Zheng, C. Chen, and X. Chu, "The effect of wall blockages on indoor small cell networks with los/nlos user association strategies," in *IEEE VTC-Spring*, pp. 1–6, 2021.

[26] T. Bai, R. Vaze, and R. W. Heath, "Using random shape theory to model blockage in random cellular networks," in *SPCOM*, pp. 1–5, 2012.